

Hyperthermia temperature reduction in biomagnetic flow: Thermal transfer in Fe_3O_4 -blood particle suspension with uniform and non-uniform effects

Cite as: Phys. Fluids **35**, 011902 (2023); <https://doi.org/10.1063/5.0128247>

Submitted: 27 September 2022 • Accepted: 14 December 2022 • Accepted Manuscript Online: 16 December 2022 • Published Online: 06 January 2023

 M. H. Faruk,  M. Ferdows and  E. E. Tzirtzilakis



View Online



Export Citation



CrossMark

ARTICLES YOU MAY BE INTERESTED IN

[Extension of Galilean invariance to uniform motions for a relativistic equation of fluid flows](#)
Physics of Fluids **35**, 013103 (2023); <https://doi.org/10.1063/5.0128422>

[Collective transport of droplets through porous media](#)
Physics of Fluids **35**, 013304 (2023); <https://doi.org/10.1063/5.0129477>

[Surface cavitation flow characterization of jet hydrofoils based on vortex identification method](#)
Physics of Fluids (2022); <https://doi.org/10.1063/5.0126564>



Physics of Fluids

Special Topic: Paint and Coating Physics

Submit Today!

Hyperthermia temperature reduction in biomagnetic flow: Thermal transfer in Fe_3O_4 -blood particle suspension with uniform and non-uniform effects

Cite as: Phys. Fluids **35**, 011902 (2023); doi: 10.1063/5.0128247
Submitted: 27 September 2022 · Accepted: 14 December 2022 ·
Published Online: 6 January 2023



View Online



Export Citation



CrossMark

M. H. Faruk,¹  M. Ferdows,^{1,a)}  and E. E. Tzirtzilakis^{2,b)} 

AFFILIATIONS

¹Research Group of Fluid Flow Modeling and Simulation, Department of Applied Mathematics, University of Dhaka, Dhaka 1000, Bangladesh

²Fluid Dynamics and Turbo-machinery Laboratory, Department of Mechanical Engineering, University of the Peloponnese, Patras, Greece

^{a)}Author to whom correspondence should be addressed: ferdows@du.ac.bd. URL: <http://ffms.du.ac.bd/mferdows/>

^{b)}URL: http://econ.uop.gr/~etzirtzilakis/English/EN_index.htm

ABSTRACT

Magnetic hyperthermia is beneficial in cancer treatment and in the treatment of some blood vessel diseases. However, excessive temperatures may also kill healthy cells in the vicinity of a sick cell. Using magnetic nanoparticles and changing the nature of the magnetic field as required, magnetic hyperthermia may be regulated in the blood. This research examines the effects of uniform and non-uniform magnetic fields on suspensions of bio-magnetic fluid and nano-bio-magnetic fluid under hyperthermia. Blood is a diamagnetic material, and when combined with superparamagnetic Fe_3O_4 , its thermo-mechanical characteristics are changed significantly. By manipulating the nature of the magnetic field, it is possible to raise or decrease the temperature in the flow domain of magnetic nano-fluids. A computational study of two such magnetic fields has been conducted, and their effects on the blood-based magneto nano-fluid flow in a rectangular conduit have been documented in this study using COMSOL multi-physics. Results indicate that a uniform magnetic field increases temperature only locally, but decreases the overall temperature in the domain. The non-uniform field of a current-carrying wire decreases both the local maximum and average blood temperature as field strength increases.

Published under an exclusive license by AIP Publishing. <https://doi.org/10.1063/5.0128247>

I. INTRODUCTION

In medical applications, the significance of magnetism cannot be overstated. With a high concentration of hemoglobin molecules, human blood is susceptible to change when exposed to a strong magnetic field.¹ Though in some kinds of the literature, blood is considered both diamagnetic and paramagnetic based on its oxidized state,² in practical consideration, blood mostly exhibits diamagnetic properties,³ which are extremely weak by nature. So, often magnetic nanoparticles (MNP) are used to improve blood's mechanical properties, such as MNPs like ferrosferric oxide (Fe_3O_4), which are widely employed for their superparamagnetic properties to influence the magnetism and thermodynamic properties of biofluids in various applications.

The most prominent uses of magnetism in medical applications are seen in magnetic resonance imaging (MRI),^{4–6} drug delivery,^{7–9}

hyperthermia,^{10–12} and cell separation.^{13,14} Diagnostic imaging revealed the importance of magnetism in medicine, but until the introduction of nanotechnology, larger applications remained unknown. When magnetic resonance imaging (MRI) made the transition from the research laboratories to the clinic, it was frequently employed to identify malignant tumors. MRI scanners provided physicians with access to the first machines capable of producing enormous magnetic fields, inspiring many to investigate how magnetism can be used for purposes other than imaging. Unfortunately, this line of investigation offered few novelties, and traditional MRI imaging remained the primary application of magnetism in medicine. When nanotechnology came into being, magnetic nanoparticles were able to convert natural tissue into magnetically sensitive material.¹⁵ This dramatically expanded the spectrum of possible medicinal uses.

Magnetic nanoparticles, which are typically very smaller in size, might be utilized to mark cells and biomolecules, thereby endowing tissues and other biological molecules with magnetic characteristics. In the near past, there has been an explosion of research aimed at creating several medicinal uses for magnetic nanoparticles. In every scenario, physical magnetic fields interacting with ferromagnetic material may connect or interact with tissue, cells, or biomolecules, hence allowing applications ranging from magnetic heating to molecular imaging. These technologies mainly depend on superparamagnetic iron oxide nanocrystals (SPIONs): these materials are made of iron oxide but, because of their tiny dimensions, they do not display magnetization until exposed to an external magnetic field.

Nanomaterials are of significant scientific interest because they serve as a link between bulk materials and atomic or molecular structures, and the properties of materials may alter as the nanoscale is approached. Nanoparticles have attracted considerable attention in recent years owing to their potential biological applications. Magnetic nanoparticles are a kind of nanoparticle that can be sent to a specific bodily site by modulating an external magnetic field. High magnetization is required for magnetic nanoparticles to respond to an externally applied magnetic field at tolerable temperatures. Iron oxide nanoparticles (Fe_3O_4) with much higher saturation magnetization values are ideal for this application. Moreover, their non-toxicity, biocompatibility, surface functionalism, and MRI contrast agents make them excellent for noninvasive diagnosis, disease detection, and therapy. Therefore, superparamagnetic (Fe_3O_4) nanoparticles are one of the most significant and well-acknowledged solutions for therapeutic applications indicated in the preceding paragraph.

Due to the immense influence on human existence, cancer treatment has received considerable attention during the last decade. The purpose of cancer therapy is to eliminate malignant cells while minimizing harm to healthy cells. It is difficult to distinguish between cancer cells and normal cells, making chemotherapy and radiation therapy less effective and replete with adverse effects. Heating therapy, also known as hyperthermia, has a great deal of potential as an adjunct cancer treatment. It is generally known that tumors have decreased blood flow, which leads to a shortage of oxygen and the development of lactic acid, which acidifies the cells. Acidic cells have lower thermal resistance than normal cells, and their capacity to disperse heat is constrained by the tumor's diminished blood flow. Therefore, elevating the local temperature between 42 and 46 °C may destroy malignant cells with some effects on healthy cells. Local hyperthermia is the process of heating a tiny target region, such as a tumor.

Since the introduction of BFD by Pai *et al.*,¹⁶ many analytical, numerical, and experimental investigations have been conducted, and BFD as an area of study has expanded significantly. Some of the previous works related to this study was reviewed by us for the development of this study. It was demonstrated by Khanafer and Vafai¹⁷ that the rise in the nano-fluid heat transfer coefficient exceeds what a conventional equation would predict. Tao and Huang¹⁸ have shown experimentally that a 1.3 T magnetic field considerably reduces blood viscosity. Researchers¹⁹ also showed that raising the volume percent of nanoparticles may either boost or decrease heat transmission. Using a Maxwell coil pair, Murase *et al.*²⁰ conducted an experiment to determine whether the temperature in magnetic hyperthermia may be regulated by an applied magnetic field and a static magnetic field. They developed an empirical equation to describe the dissipation of energy

on MNPs. Tzirtzilakis and Xenos investigated a square reservoir holding a magnetic nano-fluid that was electrically impacted by the wire's magnetic field;²¹ their findings demonstrated that the fluid influenced by the magnetism is vulnerable to this force. Under the effect of Kelvin force, vortices are created that influence the rate of heat transfer, and the size of these vortices is proportional to the intensity of the external magnetic field. Voros *et al.*²² have shown that magnetic hyperthermia is used for blood clot lysis in addition to tumor treatment. Sheikholeslami *et al.*²³ investigated a magnetic nano-fluid-filled micro-channel in the vicinity of an asymmetric magnetic field. Whenever the gradient of the magnetic field was in the same orientation as the nano-fluid flow, maximum heat transfer took place. When the magnetic field was applied in the other direction, however, heat transmission was reduced. Local electrical activity in the flow field improves thermal performance in the transition zone and has global effects on how heat moves. Tang *et al.*²⁴ performed a numerical analysis of how the non-uniformity of a solenoid's magnetic field might significantly impact the temperature distribution. In various fields of engineering and medicine, the usage of nano-fluid is on the rise owing to its superior thermal efficiency compared to the base fluid.^{25,26} Abdi *et al.*²⁷ explored MNP in a square lid-driven cavity using the same magnetic field as this study but in the turbulent flow regime. Badfar *et al.*²⁸ simulated drug targeting with the help of magnet, in blood vessel with stenosis utilizing Fe_3O_4 magnetic nanoparticles in the same kind of magnetic field. Chandrasekharan *et al.*²⁹ have shown that magnetic fluid hyperthermia is utilized to treat some blood diseases like restenosis, which is a reoccurring stenosis, in order to eliminate plaques, ablate nerves, and ease pain by boosting regional blood flow. Experiments were done by some authors to study heat transfer in a tube with a friction factor of 5 and a high Prandtl number of laminar flows.³⁰ Venkatadri showed that the effect of locations on a magnetic wire in a square enclosure is important to the effect on the fluid.³¹ As a result, nanoscale solid particles are often used in investigations and research. The findings of experiments indicate that nanoparticles improve fluid thermal conductivity owing to their high conductivity and dispersion in the base liquid, which is one of the fundamental characteristics of heat transfer.³²

Using electromagnetic theories and fluid flow, this study examines a square duct containing a magnetic nano-fluid (a mixture of water and Fe_3O_4) at varying volume fractions and magnetic numbers in the laminar flow regime under the magnetic field of an electric current-carrying wire. We also examine the effects of a uniform and non-uniform magnetic field on whole blood and blood-bearing (Fe_3O_4) particles, where a non-uniform magnetic field is produced by a current-carrying wire and the fluid has attained hyperthermia, $T_F \geq 45$. Depending on the severity of the disease, any tumor, diseased blood vessel region, or other organs where the hyperthermia process is being carried out may be subjected to a constant high temperature for an extended period. This increases the risk of damaging more neighboring cells by exposing them to very high temperatures. In cases like this, a process that reduces temperature in a specific domain becomes very useful. Our research illustrates that so can be done very efficiently if we use a non-uniform magnetic field very close to the blood vessel.

II. GEOMETRIC MODEL

Two separate perspectives are presented below for the applied magnetic field. Figures 1(a) and 1(b) depict a square duct with side h

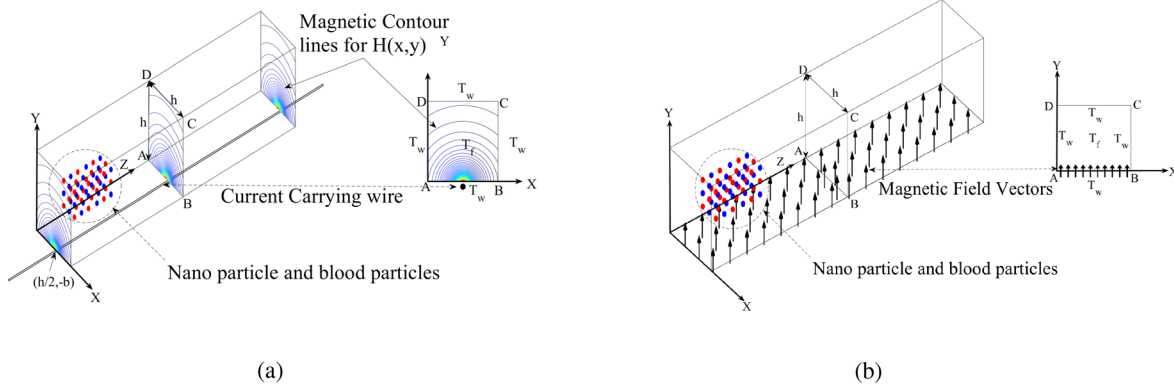


FIG. 1. Geometric model of the problem and magnetic field. (a) Non-uniform magnetic field. (b) Uniform magnetic field.

and scattered nanoparticles under the influence of a uniform and non-uniform magnetic field in two separate models. The non-uniform magnetic field is seen in Fig. 1(a), in the transverse plane of the rectangular channel. The magnetic field is produced by a wire carrying electric current. The wire is positioned along the straight line, $x = h/2, y = -b$, and the diameter of the wire is neglected so that the cross section of the wire at $z = 0$ is considered a point. In the case of Fig. 1(a), the magnetic field acts parallel to the z -plane, starting at the bottom of the xz plane; hence, only the magneto-hydrodynamic force is felt against the axial force. It happens only because the electrical conductivity of blood helps it be affected by the magnetic field. Assuming fully developed temperature and noticing that the magnetic field does not vary along the z -axis, the problem may be studied on a projection plane in the vicinity of the duct. These planes are shown in the insets of Figs. 1(a) and 1(b). In the case of uniform magnetic field, the magnetic field is represented as parallel vectors, whereas in the non-uniform one the contours of the field are given by a function that is inversely proportional to the distance from the wire to a point on the plane keeping the wire at the center below the lower wall. As the distance from the wire increases, the magnetic strength of the wire decreases. The point on the plane where the magnetic strength is the strongest is $(x, y) = (h/2, 0)$.

III. GOVERNING EQUATIONS

Without considering the cases of magnetic field, general Navier–Stokes equations for magnetic fluid in vector form² are

$$\text{Continuity equation: } \nabla \cdot \mathbf{V} = 0.$$

$$\text{Momentum equation:}$$

$$\rho \frac{D\mathbf{V}}{Dt} = -\nabla p + \rho \mathbf{F} + \mu \nabla^2 \mathbf{V} + \mathbf{J} \times \mathbf{B} + \mu_0 (\mathbf{M} \cdot \nabla) \mathbf{H}.$$

$$\text{Energy equation:}$$

$$\rho C_p \frac{DT}{Dt} + \mu_0 T \frac{\partial M}{\partial T} \frac{DH}{Dt} - \frac{\mathbf{J} \cdot \mathbf{J}}{\sigma} = k \nabla^2 T + \mu \Phi,$$

where Φ is dissipation due to viscosity, given as

$$\Phi = 2 \left\{ \left(\frac{\partial u}{\partial x} \right)^2 + \left(\frac{\partial v}{\partial y} \right)^2 + \left(\frac{\partial w}{\partial z} \right)^2 \right\} + \left(\frac{\partial v}{\partial x} + \frac{\partial u}{\partial y} \right)^2 + \left(\frac{\partial w}{\partial y} + \frac{\partial v}{\partial z} \right)^2 + \left(\frac{\partial u}{\partial z} + \frac{\partial w}{\partial x} \right)^2 - \frac{2}{3} \left(\frac{\partial u}{\partial x} + \frac{\partial v}{\partial y} + \frac{\partial w}{\partial z} \right)^2.$$

Required magnetic field equations are given as $\nabla \times \mathbf{H} = \mathbf{J} = \sigma (\mathbf{V} \times \mathbf{B})$ and $\nabla \cdot \mathbf{B} = \nabla \cdot (\mathbf{H} + \mathbf{M}) = 0$. In the momentum equation, $\mu_0 (\mathbf{M} \cdot \nabla) \mathbf{H}$ is the magnetic force due to magnetization per unit volume. Assuming that \mathbf{M} and \mathbf{H} are parallel and $M \ll H$, $\nabla \cdot \mathbf{B} = 0$, and using $\mathbf{J} = \nabla \times \mathbf{H}$, and $\mathbf{B} = \mu_0 \mathbf{H}$, it can be showed³³ that $\mu_0 (\mathbf{M} \cdot \nabla) \mathbf{H} = \mu_0 M \nabla H + \mathbf{J} \times \mathbf{B}$. Given that $B = B(x, y)$, the Lorentz force term in momentum equations is as follows: $\mathbf{J} \times \mathbf{B} = \{ \sigma B_y (v B_x - u B_y), \sigma B_x (u B_y - v B_x), -\sigma w B^2 \}$. Joule heating term in temperature equation is $\mathbf{J} \cdot \mathbf{J} = \sigma^2 ((w B)^2 + (u B_y - v B_x)^2)$. Assuming fully developed flow, that is, $\frac{\partial u}{\partial z} = \frac{\partial v}{\partial z} = \frac{\partial w}{\partial z} = 0$ and fully developed temperature, that is, $\frac{\partial T}{\partial z} = 0$ along the axial direction, and also considering that the axial pressure gradient is constant or $\frac{\partial p}{\partial z} = -P_z$ and finally by the assumption of saturated magnetization, we have $\frac{\partial M}{\partial T} = 0$. Then, with a non-uniform magnetic field $H(x, y)$ and internal magnetization function M , governing equations for velocity components u, v, w , temperature T , and pressure p is taken as Tzirtzilakis³⁴ and Mousavi³⁵ with the addition of the energy equation as

$$\begin{aligned} \rho C_p \left(\frac{\partial T}{\partial t} + u \frac{\partial T}{\partial x} + v \frac{\partial T}{\partial y} \right) &= \sigma w^2 B^2 - \sigma (B_y u - B_x v)^2 \\ &\quad - \mu_0 T \frac{\partial M}{\partial T} \left(u \frac{\partial H}{\partial x} + v \frac{\partial H}{\partial y} \right) \\ &\quad + k \left(\frac{\partial^2 T}{\partial x^2} + \frac{\partial^2 T}{\partial y^2} \right) + \mu \Phi, \end{aligned}$$

where Φ is given as

$$2 \left\{ \left(\frac{\partial u}{\partial x} \right)^2 + \left(\frac{\partial v}{\partial y} \right)^2 \right\} + \left(\frac{\partial u}{\partial y} + \frac{\partial v}{\partial x} \right)^2 + \left(\frac{\partial w}{\partial x} \right)^2 + \left(\frac{\partial w}{\partial y} \right)^2,$$

and boundary conditions as at $y = 0$ or h and $0 \leq x \leq h$ $u = 0$ $v = 0$ $w = 0$ $T = T_w$ at $x = 0$ or h and $0 \leq y \leq h$ $u = 0$ $v = 0$ $w = 0$ $T = T_w$. Here, ρ, μ, σ and μ_0 are, respectively, density, viscosity, electric conductivity, and magnetic permittivity of the fluid. When we assume a uniform magnetic field, magnetic field strength \mathbf{H} does not change in any direction and works parallel to y direction. So, $\frac{\partial H}{\partial z} = 0$ as before. However, this time components H_x and H_y become zero too. The components of Lorentz force given in momentum and temperature equation are, respectively, $\mathbf{J} \times \mathbf{B} = \{0, 0, -\sigma w B^2\}$ and

$\mathbf{J} \cdot \mathbf{J} = \sigma^2 (wB)^2$. In this study, we also use a magnetic field generated by a current carrying wire, given as

$$H(x, y) = \frac{\gamma}{2\pi} \frac{1}{\sqrt{(x-a)^2 + (y-b)^2}},$$

where γ is the current passing through the wire, and the components of $H(x, y)$ are given as

$$H_x(x, y) = -\frac{\gamma}{2\pi} \frac{y-b}{\sqrt{(x-a)^2 + (y-b)^2}},$$

$$H_y(x, y) = \frac{\gamma}{2\pi} \frac{x-a}{\sqrt{(x-a)^2 + (y-b)^2}},$$

where (a, b) is the point of application for the wire or the center of the magnetic field.

There are a few empirical equations for the internal magnetization M available in the literature. For the case without any magnetic nanoparticle, we use the magnetization equation as given in Ref. 36: $M = K'H(T_c - T)$.

We find the dimensionless equation by using

$$x^* = \frac{x}{h}, \quad y^* = \frac{y}{h}, \quad z^* = \frac{z}{h},$$

$$u^* = \frac{u}{w_0}, \quad v^* = \frac{v}{w_0}, \quad w^* = \frac{w}{w_0},$$

$$H^* = \frac{H}{H_0}, \quad H_x^* = \frac{H_x}{H_0}, \quad H_y^* = \frac{H_y}{H_0},$$

$$t^* = \frac{tw_0}{h}, \quad p^* = \frac{p}{\rho w_0^2}, \quad T^* = \frac{T - T_w}{T_f - T_w},$$

and after removing the asterisk(*) sign, momentum and energy equations reduce to

$$\frac{\partial u}{\partial t} + u \frac{\partial u}{\partial x} + v \frac{\partial u}{\partial y} = -\frac{\partial p}{\partial x} + \frac{1}{\text{Re}} \left(\frac{\partial^2 u}{\partial x^2} + \frac{\partial^2 u}{\partial y^2} \right)$$

$$+ \text{Mn}_F H \frac{\partial H}{\partial x} + \text{Mn}_M (vH_x H_y - uH_y^2),$$

$$\frac{\partial v}{\partial t} + u \frac{\partial v}{\partial x} + v \frac{\partial v}{\partial y} = -\frac{\partial p}{\partial y} + \frac{1}{\text{Re}} \left(\frac{\partial^2 v}{\partial x^2} + \frac{\partial^2 v}{\partial y^2} \right)$$

$$+ \text{Mn}_F H \frac{\partial H}{\partial y} + \text{Mn}_M (uH_x H_y - vH_y^2),$$

$$\frac{\partial w}{\partial t} + u \frac{\partial w}{\partial x} + v \frac{\partial w}{\partial y} = P_z + \frac{1}{\text{Re}} \left(\frac{\partial^2 w}{\partial x^2} + \frac{\partial^2 w}{\partial y^2} \right) - \text{Mn}_M w H^2,$$

$$\frac{\partial T}{\partial t} + u \frac{\partial T}{\partial x} + v \frac{\partial T}{\partial y} = \text{Ec} \text{Mn}_M \sigma (w^2 B^2 + (B_y u - B_x v)^2)$$

$$+ \frac{1}{\text{Pr} \text{Re}} \left(\frac{\partial^2 T}{\partial x^2} + \frac{\partial^2 T}{\partial y^2} \right),$$

$$+ \frac{2\text{Ec}}{\text{Re}} \left[\left\{ \left(\frac{\partial u}{\partial x} \right)^2 + \left(\frac{\partial v}{\partial y} \right)^2 \right\} \right]$$

$$+ \left(\frac{\partial u}{\partial y} + \frac{\partial v}{\partial x} \right)^2 + \left(\frac{\partial w}{\partial x} \right)^2 + \left(\frac{\partial w}{\partial y} \right)^2$$

with boundary condition at $y = 0$ or 1 and $0 \leq x \leq 1$ $u = 0$ $v = 0$ $w = 0$ $T = 0$ at $x = 0$ or 1 and $0 \leq y \leq 1$ $u = 0$ $v = 0$ $w = 0$ $T = 0$, where $\text{Re} = \frac{\rho h w_0}{\mu}$, $\text{Pr} = \frac{C_p \mu}{k}$, $\text{Ec} = \frac{w_0^2}{C_p (T_f - T_w)}$,

$$\text{Mn}_F = \frac{\mu_0^2 H_0^2 K' (T_f - T_w)}{\mu_0 \rho w_0^2}$$

$$= \begin{cases} \frac{B_0^2 K' (T_f - T_w)}{\mu_0 \rho w_0^2} & \text{reaching a constant temperature,} \\ \frac{B_0 M_s}{\rho w_0^2} & \text{saturation magnetization,} \end{cases}$$

$$\text{Mn}_M = \frac{\sigma h \mu_0^2 H_0^2}{\rho w_0} = \frac{\sigma h B_0^2}{\rho w_0} = \frac{\text{Ha}^2}{\text{Re}} = \text{N}.$$

The relation given here for Mn_F and Mn_M is generally true for calculation related to pure blood. Mn_F will change in the case of Fe_3O_4 -blood suspension according to the magnetization scheme of Langevin model.

Now in our first case of non-uniform magnetic field, we consider blood as a standalone biomagnetic fluid, where we have two considerations: first, we consider that the change of M with respect to T is negligible,² that is, $\frac{\partial M}{\partial T} \sim 0$, and second, we consider that the fluid has reached complete saturation point, and thus, $M = M_0$ and $\frac{\partial M}{\partial T} = 0$. In the second case, $\text{Mn}_F = \frac{B_0 M_s}{\rho w_0^2}$ and the term due to FHD will change to $\text{Mn}_F H \frac{\partial H}{\partial x}$ and $\text{Mn}_F H \frac{\partial H}{\partial y}$ in momentum and energy equations. Both cases remove the heating term due to internal magnetization, and thus, a flow profile is obtained, where the temperature profile is controlled by the velocity, joule heating term, and dissipation term only.

For the case with the ferro-fluid, we measure the nano-fluid properties ($\Pi = \rho, C_p, \rho C_p$) of ferro-fluid with the help following formula: $\Pi_{\text{mnp}} = (1 - \phi) \Pi_{\text{blood}} + \phi \Pi_{\text{Fe}_3\text{O}_4}$ and effective viscosity is adapted as³⁷ $\mu_{\text{mnp}} = \frac{\mu_{\text{blood}}}{(1 - \phi)^{2.5}}$, considering that the nanoparticles are spherical, and effective heat conduction co-efficient is given as³⁸

$$k_{\text{mnf}} = \frac{k_{\text{Fe}_3\text{O}_4} + 2k_{\text{blood}} - 2(k_{\text{blood}} - k_{\text{Fe}_3\text{O}_4})}{k_{\text{Fe}_3\text{O}_4} + 2k_f + \phi(k_f - k_{\text{Fe}_3\text{O}_4})}.$$

Effective electrical conductivity is given as³⁹

$$\sigma_{\text{mnf}} = \left\{ 1 + \frac{3 \left(\frac{\sigma_{\text{Fe}_3\text{O}_4} - 1}{\sigma_{\text{blood}}} \right) \phi}{\left(\frac{\sigma_{\text{Fe}_3\text{O}_4}}{\sigma_{\text{blood}}} + 2 \right) - \left(\frac{\sigma_{\text{Fe}_3\text{O}_4}}{\sigma_{\text{blood}}} - 1 \right) \phi} \right\} \sigma_{\text{blood}}.$$

In the case of magnetic nano-fluid, the magnetic field remains the same, but unlike whole blood, now we consider another magnetization formula known as Langevin magnetization model in the literature, given as $M_l = M_s \left\{ \coth(\xi) - \frac{1}{\xi} \right\}$, where $\xi = \frac{\mu_0 m H}{k_B T}$ and $M_s = nm = \phi M_d$

This model of magnetization is considered because of the use of particle parameters in the equation. For this reason, in the literature it is often associated with nanoparticle that gets affected by magnetization of a magnetic field.

Due to the presence of coth and reciprocal of ξ , $L(\xi)$ is a non-linear function of ξ . So, we use different approximations of $L(\xi)$ based on low-order series approximation of $L(\xi)$ about $\xi = 0$. For weak

magnetization, we use the fact that $L(\xi) \sim \frac{\mu_0 m H}{3k_B T}$, which after using non-dimensional variables becomes, $L(\xi) \sim \frac{\mu_0 m}{3k_B} \frac{H_0}{T_f - T_w} \frac{H^*}{T^* + \varepsilon}$, and consequently, $\frac{\partial M}{\partial T} \sim M_s \left(-\frac{\mu_0 H}{3k_B T^2}\right)$.

So, the term in the energy equation becomes

$$\mu_0 T \frac{\partial M}{\partial T} \sim \mu_0 M_s \left(-\frac{\mu_0 m H}{3k_B T}\right) \sim \mu_0 M_s \left(-\frac{\mu_0 m}{3k_B} \frac{H_0}{T_f - T_w} \frac{H^*}{T^* + \varepsilon}\right).$$

Thus, in this case, we use $Mn_{\text{blood_mnp}} = \frac{mM_s \mu_0^2 H_0^2}{3k_B(T_f - T_w)w_0^2 \rho} = \frac{mM_s B_0^2}{3k_B(T_f - T_w)w_0^2 \rho}$, for which FHD terms in the momentum equations for MNP will carry, respectively,

$$Mn_{\text{blood_mnp}}(1 - T)H \frac{\partial H}{\partial x} \text{ and } Mn_{\text{blood_mnp}}(1 - T)H \frac{\partial H}{\partial y},$$

and in the energy equation, we will have $-Ec_{\text{mnp}}Mn_{\text{blood_mnp}} \times (T + \varepsilon)H \left(u \frac{\partial H}{\partial x} + v \frac{\partial H}{\partial y}\right)$.

For strong magnetization, when $\xi \rightarrow \infty$, $\text{coth}(\xi) \rightarrow 1$ so,

$$L(\xi) \sim 1 - \frac{1}{\xi} = 1 - \frac{k_B T}{\mu_0 m H}$$

and $\frac{\partial M}{\partial T} \sim M_s \left(-\frac{k_B}{\mu_0 m H}\right)$.

Consequently, $\mu_0 T \frac{\partial M}{\partial T} \sim \mu_0 M_s \left(-\frac{k_B T}{\mu_0 m H}\right) \sim \mu_0 M_s \left(-\frac{k_B}{\mu_0 m} \frac{T_f - T_w T + \varepsilon}{H_0} \frac{H^*}{H}\right)$. Due to the presence of $T + \varepsilon$, we get two non-dimensional number from this case that arise in FHD, and they are

$$Mn_{F_{\text{mnp}1}} = \frac{M_s [k_B(T_f - T_w)]}{mw_0^2 \rho}$$

and

$$Mn_{F_{\text{mnp}2}} = \frac{M_s(m\mu_0 H_0)}{mw_0^2 \rho} = \frac{M_s(\mu_0 B_0)}{mw_0^2 \rho}.$$

Consequently, magnetization forces in momentum equations are

$$-Mn_{F_{\text{mnp}1}} \frac{T + \varepsilon}{H} \frac{\partial H}{\partial x} + Mn_{F_{\text{mnp}2}} \frac{\partial H}{\partial x}$$

and

$$-Mn_{F_{\text{mnp}1}} \frac{T + \varepsilon}{H} \frac{\partial H}{\partial y} + Mn_{F_{\text{mnp}2}} \frac{\partial H}{\partial y},$$

respectively, in the x and y momentum directions.

For the FHD term in energy equation,

$$-Ec_{\text{mnp}}Mn_{F_{\text{mnp}1}} \frac{T + \varepsilon}{H} \left(u \frac{\partial H}{\partial x} + v \frac{\partial H}{\partial y}\right).$$

A magnetic field is saturated when with the increase in magnetic field, the magnetization value M_s does not change. When we consider complete saturated magnetization from $t = 0$, then $M_L = M_s$. Therefore, $Mn_{F_{\text{mnp}2}}$ remains but $Mn_{F_{\text{mnp}1}}$ vanishes, and also, $\frac{\partial M}{\partial T} = 0$ is considered like before. This is the case in Fig. 2 where the $L(\xi)$ converges to the line $y = 1$. In the case of complete saturation, we consider that the saturation was reached in the weak magnetic strength range. It is also to be noted that, when the field is saturated, B_0 value changes with H but not the value of M . Langevin function or any other function given for the magnetization is generally an empirical formula.

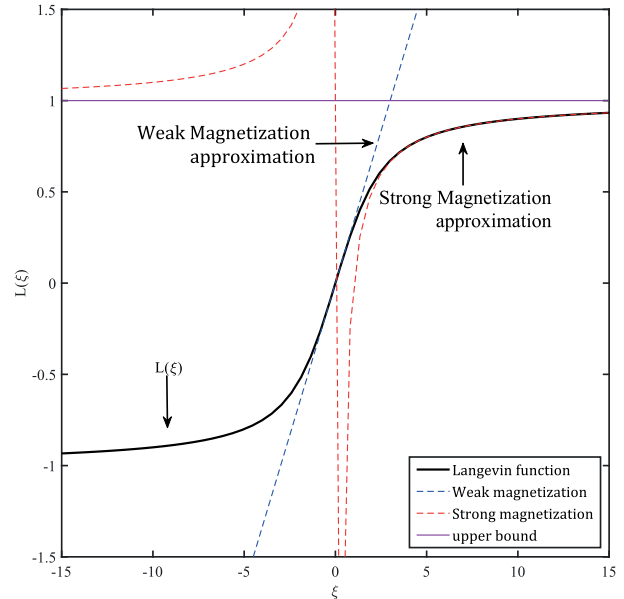


FIG. 2. Langevin magnetization approximation.

They were formulated by different scientists as an outcome of physical experiment. Figure 2 shows different approximations of $L(\xi)$ discussed above.

IV. DOMAIN DISCRETIZATION AND SIMULATION

As seen in Figs. 3(a) and 3(b), we generated a mesh for the analysis of a uniform magnetic field. Our computational domain is a basic square plane projected from a long rectangular conduit with a square inlet and exit. We developed a domain-specific structured mesh. In Fig. 3(a), the mesh is not uniform over the whole domain. We deliberately make it denser at the edges by adding a factor of exponential growth of 5 for a 150×150 grid.

For the non-uniform magnetic field, an additional change is required such that for a 200×200 grid, the mesh on both sides of the midline $x = 0.5$ and the four boundaries are denser [as shown in Fig. 3(b)], as is the current-carrying wire slightly below the x axis along $x = 0.5$. Therefore, the force of the magnetic field is particularly strong close to that point and at locations that are vertically parallel. The change in force along $x = 0.5$ is disproportionately large compared to the change in distance x . So, the exponential growth factor is 10 on the upper, lower, and on $x = 0.5$ line, whereas on the right and left boundary, we keep it at 5.

We use the COMSOL multiphysics software for the simulation of the study. The PDE interface of Mathematics module of COMSOL contains a powerful tool to find numerical solution where we define the problem in coefficient form PDE. Equation in this module is given as⁴⁰

$$e_a \frac{\partial^2 \mathbf{u}}{\partial t^2} + d_a \frac{\partial \mathbf{u}}{\partial t} + \nabla \cdot (-c \nabla \mathbf{u} - \alpha \mathbf{u} + \gamma) + \beta \cdot \nabla \mathbf{u} + a \mathbf{u} = f,$$

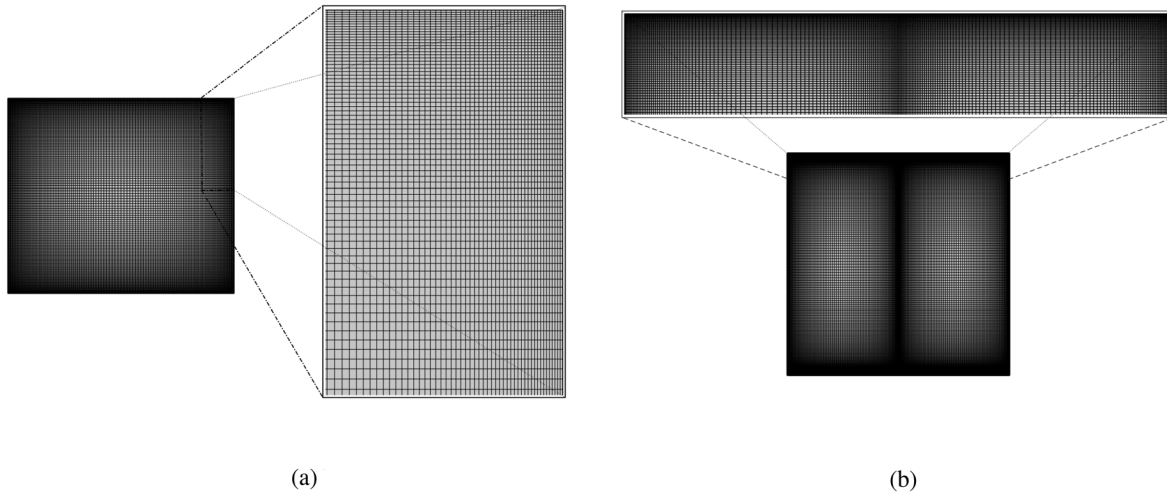


FIG. 3. Generated mesh for two magnetic fields. (a) Uniform magnetic field. (b) Non-uniform magnetic field.

where \mathbf{u} is the solution vector as $\mathbf{u} = \{u, v, w, p, T, \Psi\}^{\text{transpose}}$, t is time, and ∇ is the two-dimensional differential operator, $\nabla = \left\{ \frac{\partial}{\partial x}, \frac{\partial}{\partial y} \right\}$. \mathbf{e}_a is mass coefficient, \mathbf{d}_a is damping or mass coefficient, \mathbf{c} is diffusion coefficient, $\boldsymbol{\alpha}$ is conservative flux convection coefficient, $\boldsymbol{\gamma}$ is conservative flux source, $\boldsymbol{\beta}$ is convection coefficient, and \mathbf{a} is absorption coefficient.

In the solution \mathbf{u} , u, v, w, p, T have usual meaning and Ψ is the streamline whose Poisson equation is solved to find out the tangential streamlines of the flow. The equation is given as $\frac{\partial^2 \Psi}{\partial x^2} + \frac{\partial^2 \Psi}{\partial y^2} = -\left(\frac{\partial v}{\partial x} - \frac{\partial u}{\partial y}\right)$, with boundary condition, $\Psi = 0$ on all boundaries.

For the solution of the flow under non-uniform magnetic field, all the coefficients are given in the tensor form. For lack of relevant terms, we have $e_{aij} = 0; \alpha_{ijx} = \alpha_{ijy} = 0; a_{ij} = 0$. As the flow is fully developed, we can assume u and v are very small. Average u and v remain small so that the flow does not cross the laminar state. In that case, the terms $Mn_F H \frac{\partial H}{\partial x}$ and $Mn_F H \frac{\partial H}{\partial y}$ dominate the momentum equation with the transverse pressure gradients. Assuming that u and v are small, we have $\frac{\partial p}{\partial x} \sim Mn_F H \frac{\partial H}{\partial x}$ and $\frac{\partial p}{\partial y} \sim Mn_F H \frac{\partial H}{\partial y}$. So, we define the initial guess pressure to be $p(x, y) = \frac{1}{2} Mn_F H^2$. COMSOL multi-physics solves a PDE using finite element method. In the module setting, we use Lagrange type shape function of quadratic order to solve for our PDE.

A. Study parameters

For both types of magnetic conditions, the study was performed with a high axial pressure gradient $\frac{\partial p}{\partial z}$, 80–900 Pa/m, as found in Ref. 42, which non-dimensionally varies from 200 to 2000. We combine it with changing Re from 50 to 200. We consider a square plane of side, $h = 0.01$ m, and the characteristic velocity of blood is taken to be $w_0 = 2 \times 10^{-3}$ m/s. Universally known value of μ_0 is $4\pi \times 10^{-7}$ N/A². Also, Boltzmann constant, K_B , is given as 1.38×10^{-23} J/K. MnM was calculated, respectively, from B_0 for 0–10 T using $Mn_M = \frac{h\sigma\mu_0^2 H_0^2}{w_0\rho} = \frac{\sigma h B_0^2}{\rho w_0}$. Here, electrical conductivity $\sigma = 0.8$

siemens for blood. For the non-uniform magnetic field calculation, we adapted different parameters from Ref. 2. The non-dimensional value of $(a, b) = (0.5, -0.05)$, which is the position of the wire under the duct as in Fig. 1(a). The value of saturated magnetization of blood is taken to be $M_s = 60$ (A/m) as mentioned in Ref. 34 at $B_0 = 8$ T. Each Fe₃O₄ crystal has an approximate volume of 730 \AA^3 and contains eight molecules. Each nanoparticle includes roughly 6×10^3 molecules, each of which has a magnetic torque of $4\mu_B$.⁴³ μ_B momentum spin of a free electron of 9.27×10^{-24} m² is referred to as magneton Bohr. The magnetic torque of Fe₃O₄ nanoparticles can be calculated according to Ref. 44

$$m_0 = \frac{4\mu_B \pi d_p^3}{6 \times 91.25 \times 10^{-30}}$$

The temperature condition is very vital to the study. We consider that the wall of the duct is always at constant, $T_w = 37^\circ\text{C}$ temperature, and the fluid temperature has reached the generally accepted minimum hyperthermia temperature, that is, $T_f = 45^\circ\text{C}$. Important physical properties are tabulated in Table I.

V. RESULTS AND DISCUSSION

After the numerical solution was found, we used both COMSOL and MATLAB for the post-processing of results. For the validation of

TABLE I. Physical properties of model components.

Property	Symbol	Blood ³⁶	Fe ₃ O ₄ ⁴¹
Density (kg/m ³)	ρ	1050	5200
Conductivity [W/(m K)]	k	0.5	6
Specific heat [J/(kg K)]	C_p	3900	670
Kinematic viscosity (m ² /s)	ν	0.003	...
Diameter (m)	d_p	...	1×10^{-9}
Electrical conductivity (S/m)	σ	0.8	25 000

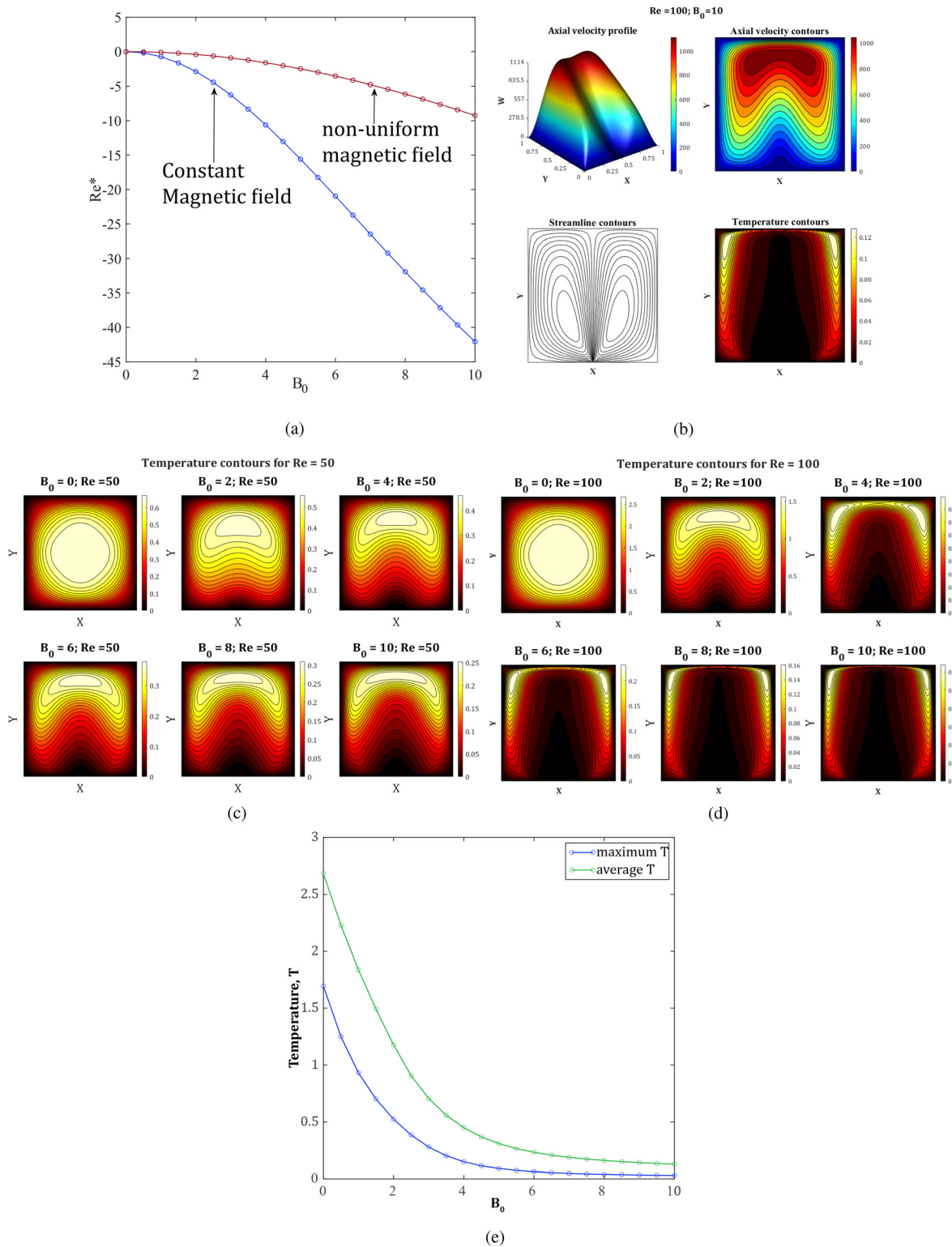


FIG. 4. Validation and nature of thermal transfer for pure blood under saturated magnetization. (a) Re^* vs B_0 . (b) Velocity profile, velocity contour, streamlines, and isotherm. (c) Change in isotherms with B_0 when $Re = 50$. (d) Change in isotherms with B_0 when $Re = 100$. (e) Maximum and average temperature for pure blood.

$Re = 250; B_0 = 10$

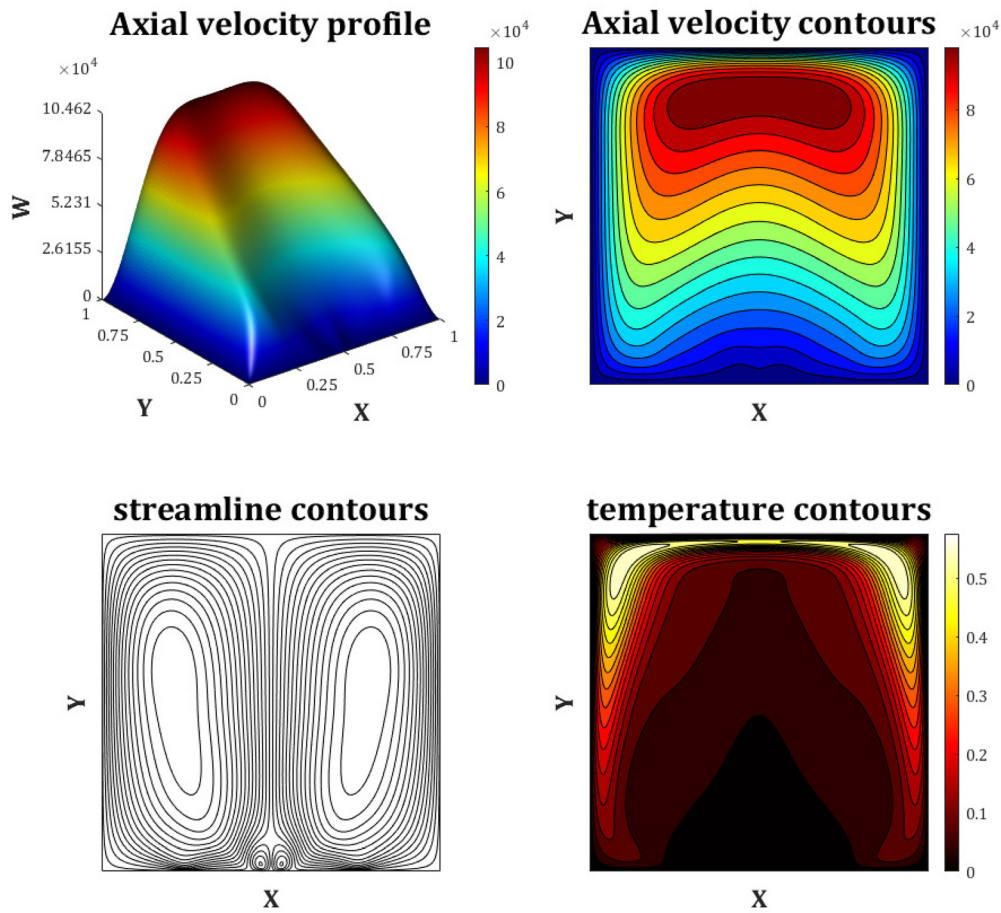


FIG. 5. Nature of flow and thermal transfer at $Re = 250$ and $B_0 = 10$ under strong magnetization for Fe_3O_4 -blood suspension.

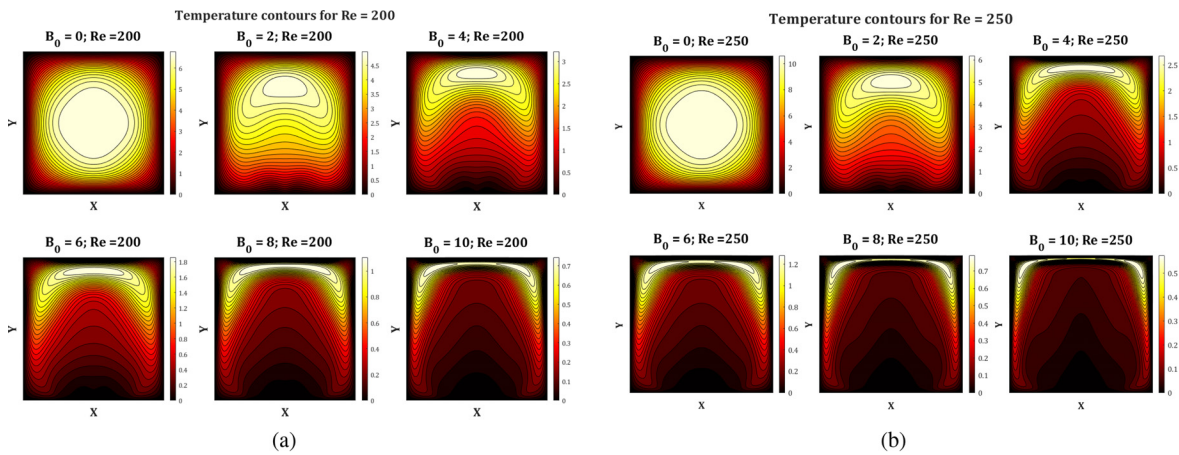


FIG. 6. Nature of thermal transfer under strong magnetization for Fe_3O_4 -blood suspension. (a) Change in isotherms with B_0 when $Re = 200$. (b) Change in isotherms with B_0 when $Re = 250$.

our computation model of both uniform and non-uniform magnetic field, we plot the graph of R^* vs B_0 as in Ref. 2, where $Re^* = \frac{Re-Re_0}{Re_0} \times 100\%$, which is the percent change of a local Reynolds number and Re_0 is the Reynolds number for $Mn_M = Mn_F = 0$. Both the figures show agreement with the data of Tzirtzilakis (with $\frac{\partial p}{\partial z} = -15\,000$).

A. Study of non-uniform magnetic field

Blood in non-uniform magnetic field was studied extensively by Tzirtzilakis.² They formed a model based on both MHD and FHD. For the validation of our study, we draw the axial velocity profile, axial velocity contour, streamline $\Psi(x, y)$, and isotherms in Fig. 4(b). The first three plots in Fig. 4(b) show qualitative agreement with the one in Ref. 2, and the last one is the output of our study. The first two plot in Fig. 4(b) shows how the magnetic force

pushes the parabolic flow profile from the lower plane of the duct and creates a dent. The streamline contour in Fig. 4(b) shows how u, v velocity components build two secondary flow region so that the axial velocity is affected from the below. For blood in saturated magnetization condition, the isotherms are given in Figs. 4(c) and 4(d) for $Re = 50$ and $Re = 100$, respectively. The isotherms show how the change in magnetic strength can cause the isotherm to bend in along the vertical midline region. Also, it shows that the intensity of this change is more for the case where the Reynolds number is greater, which shows that for a less viscous resistance the magnetic force will reduce the high-temperature region more quickly along the midline for a small magnetic field strength. This is significant because previous study shows that blood is more likely to be less viscous as the magnetic strength increases.¹⁸ Also, the temperature is higher when Re is greater or equivalently it can be said that when the viscous resistance is less.

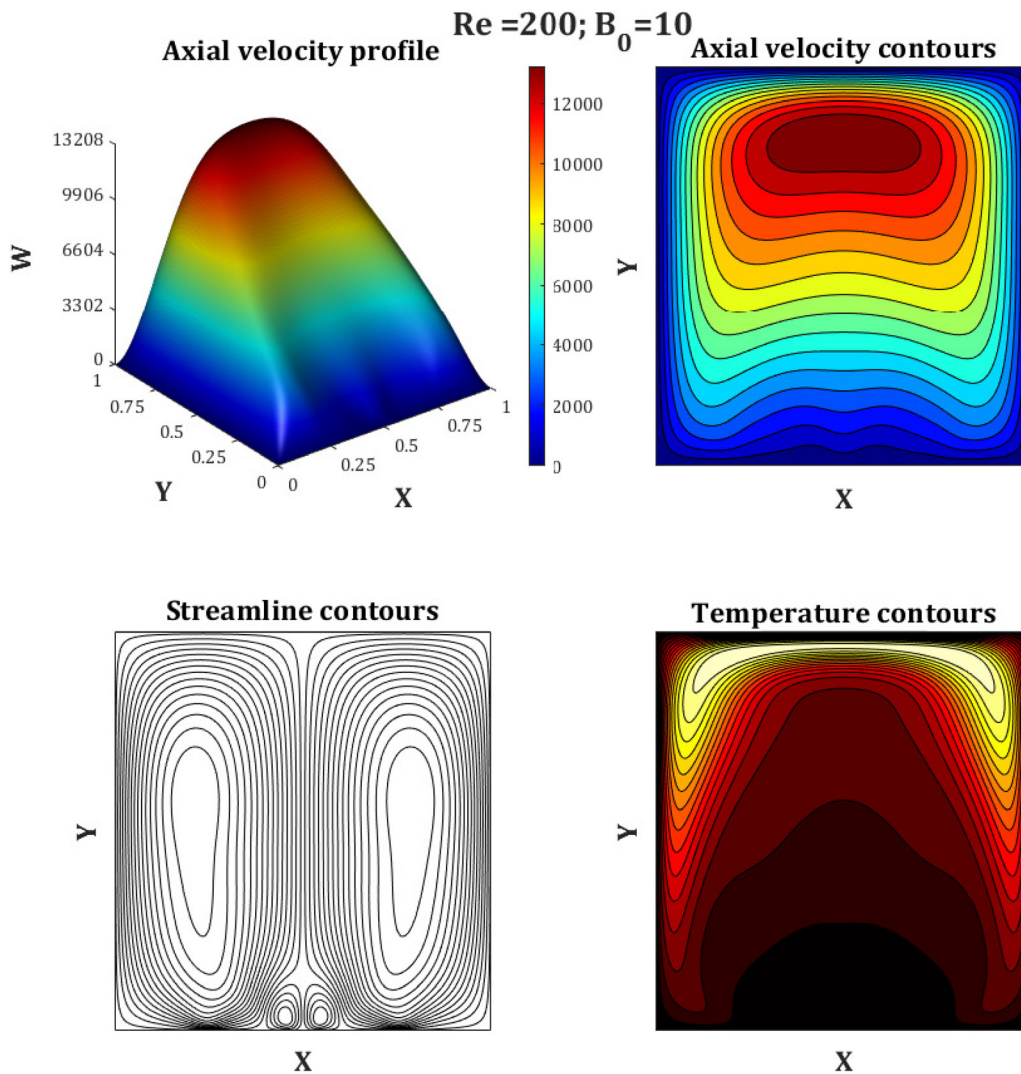


FIG. 7. Nature of flow and thermal transfer at $Re = 200$ and $B_0 = 10$ under saturated magnetization for Fe_3O_4 -blood suspension.

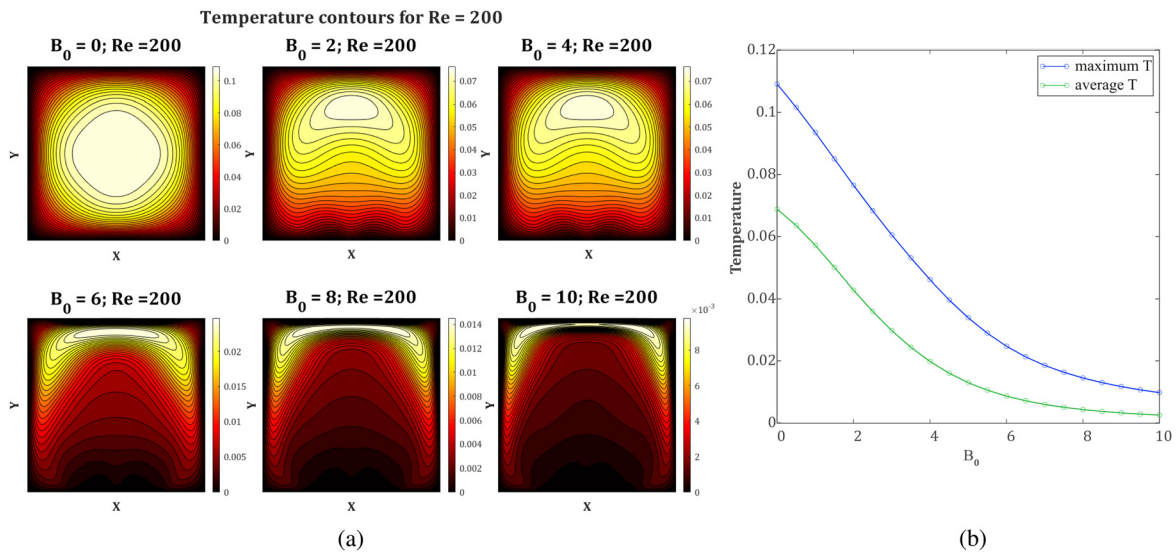


FIG. 8. Nature of thermal transfer under saturated magnetization for Fe₃O₄–blood suspension. (a) Change in isotherms with B₀ when Re = 200. (b) Maximum and average temperature for Fe₃O₄–blood suspension.

In Fig. 4(e), we see that unlike uniform magnetic field, both the maximum temperature and the average temperature decrease with the magnetic field strength. Both the values go to wall temperature as the temperature increases. Also, it is noticeable that for a B₀ of less than 2 Tesla, maximum value of T remains at hyperthermic temperature region and average temperature remains in hyper-thermal region for a slightly greater value than 0 Tesla.

In Fig. 5, we see that the velocity change is much less compared to the whole blood, but the change in temperature is still very noticeable. Also, there is now two new secondary flow region near the wire. We also simulated for the weak magnetization assumption. The result for all Langevin approximation remains qualitatively same with only

difference visible in the numerical values. For that reason, we only show here some plots for strong magnetization and saturated magnetization, and for weak magnetization, it is not repeated.

In Figs. 6(a) and 6(b), the change with the Reynolds number is very similar to the whole blood case. In a higher Reynolds number, the change in isotherm is much quicker because of the less viscous resistance.

In Fig. 7, we see that the velocity change is very small compared to whole blood, but the temperature change is still very noticeable at Re = 200 and high axial pressure gradient with high magnetic field strength. There is two new secondary flow regions near the wire in the tangential streamline of the flow as in the strong magnetization

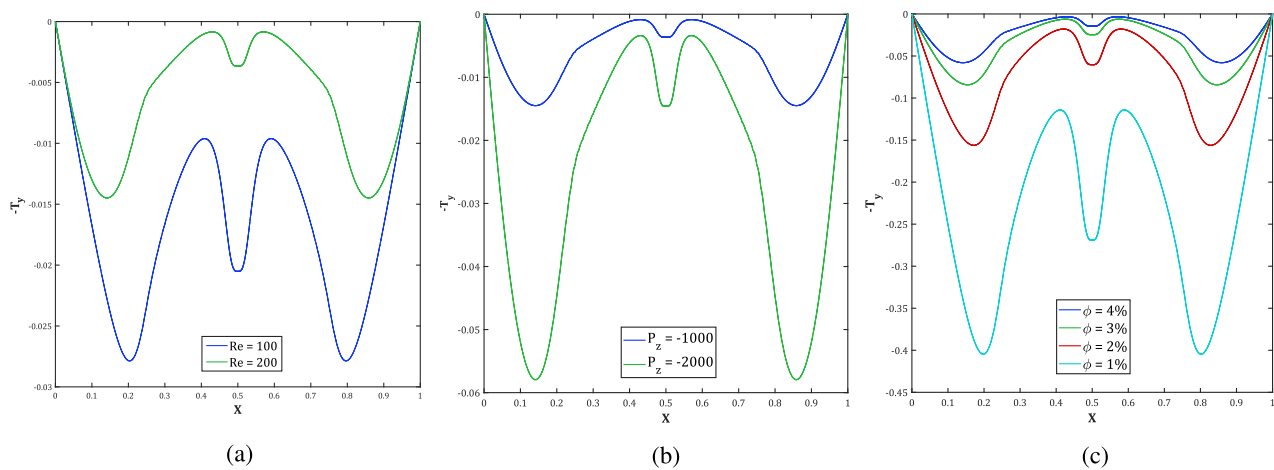


FIG. 9. Convection due to advection and diffusion proportional to $-\frac{\partial T}{\partial y} |_{y=0}$. (a) Change in nature of convection for Re. (b) Change in nature of convection for P_z. (c) Change in nature of convection for ϕ .

approximation. So, in this case, we have high velocity and diffusion of temperature. Other than that the graphs are qualitatively similar to one another. In Fig. 8(a), we see that unlike whole blood there is a two-way movement of the blood–nano-fluid mixture. The relatively higher temperature is pushed away, but also there is low temperature region, which pulls the isotherm toward the magnetic force source. In Fig. 8(b), the trend of T_{\max} and T_{avg} is same as the whole blood case, except this time the temperature remain very close to the wall temperature. For the mixed fluid in saturated magnetization, the convection coefficient or the Nusselt number will be proportional to $-\frac{\partial T}{\partial y}$ at the lower wall. So, to have an idea of the convection due to advection and conduction, we plot $-\frac{\partial T}{\partial y}$ vs Re , P_z , and ϕ , respectively, in Figs. 9(a)–9(c). It is observed that $-\frac{\partial T}{\partial y}$ increases or decreases when Re , P_z , and ϕ increase or decrease. From this, we can say that the vertical convection will be inversely proportional viscosity and directly to the volume fraction

of the particle as blood is more likely to be less viscous in a magnetic field. So, convection transfer will overall increase in blood when ϕ and P_z remain constant.

B. Study of uniform magnetic field

For uniform magnetic field, we plot the graph showing the trend of maximum temperature changing as we increase the magnetic field strength in the domain in Fig. 10(a) and for average temperature in Fig. 10(b). This two properties show contrasting behavior. The maximum temperature keeps increasing for higher magnetic strength, whereas the average temperature starts decreasing after a short constant trend. From the fully developed temperature profile, it becomes apparent that the maximum temperature value only increases locally, but the temperature profile keeps shrinking in that they move away from the wall to the center of the duct.

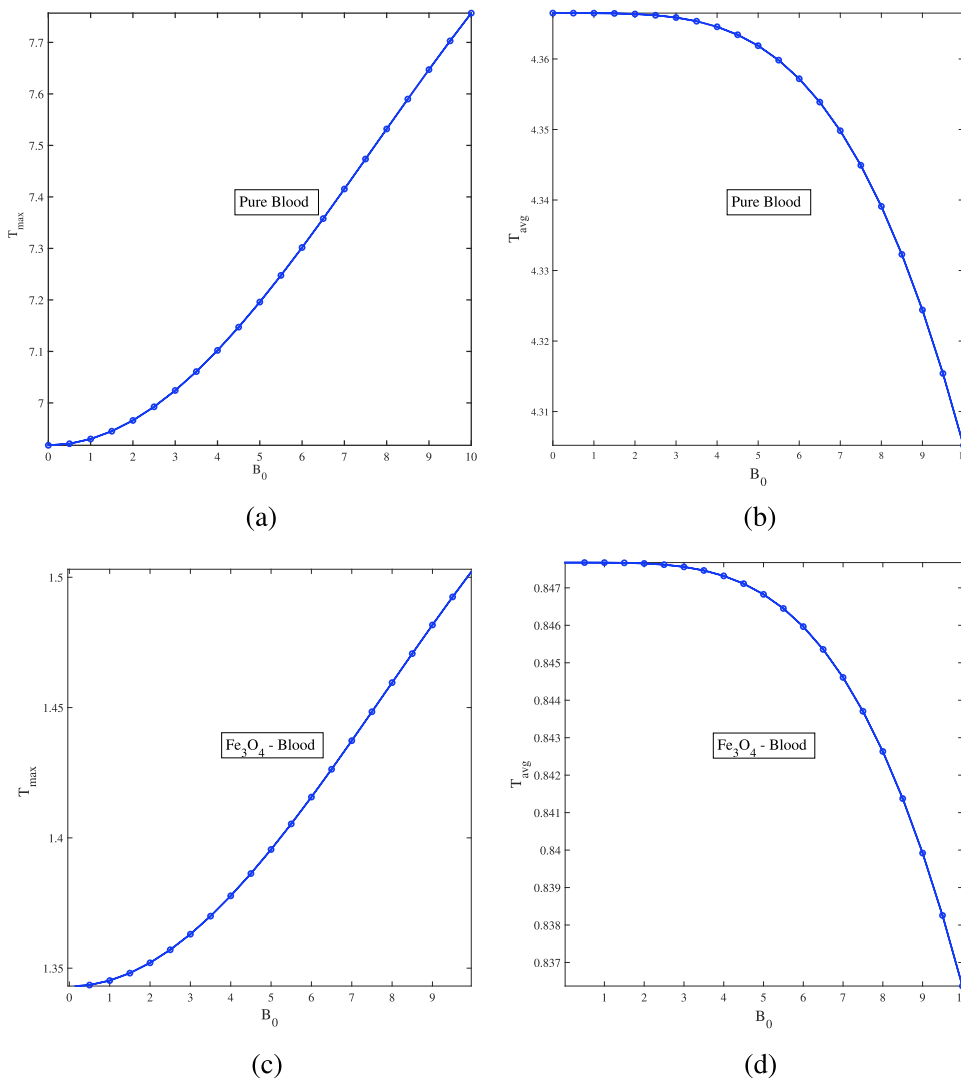


FIG. 10. Change of maximum and average temperature under uniform magnetic field. (a) Maximum T in pure blood. (b) Average T in pure blood. (c) Maximum T in Fe_3O_4 -blood. (d) Average T in Fe_3O_4 -blood.

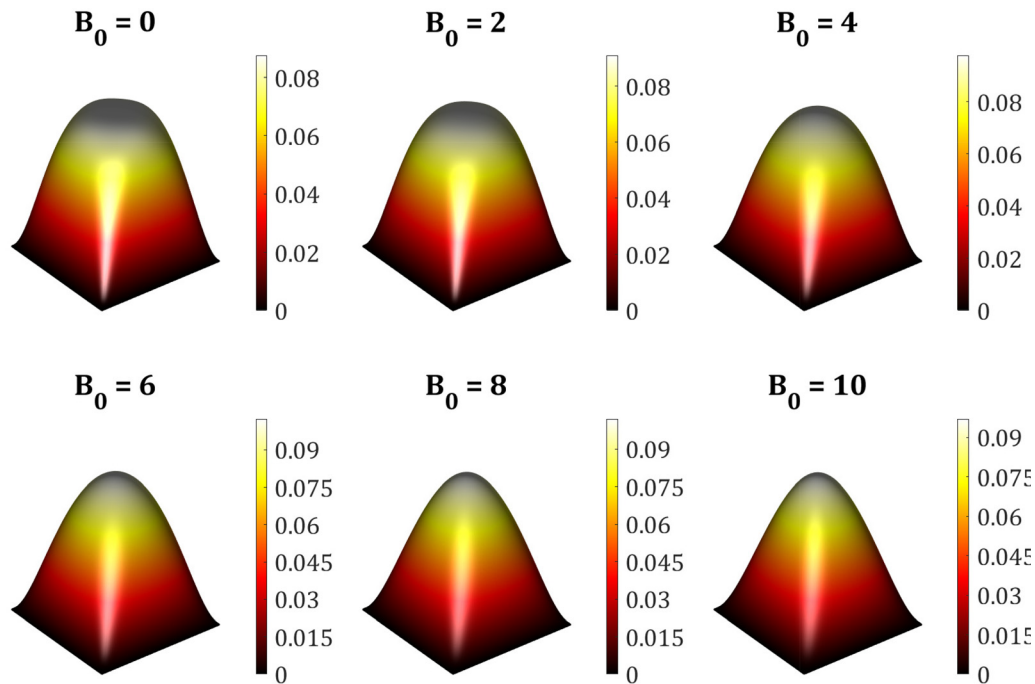


FIG. 11. Developed temperature profile in uniform magnetic field.

For Fe_3O_4 -blood suspension, we see a similar situation, but in this case, the maximum temperature remains just above the hyperthermia temperature, as can be seen in Fig. 10(c). On the other hand, the average temperature has similar trend, but the temperature is always under the hyperthermia range. Figure 10(d) shows that the average temperature is in the range $0.82 < T_{avg} < 0.85$. Both these happen for the same reason. If we look at the developed temperature profile, then we will see that the tip of the profile gets sharper, which corresponds to the increasing maximum temperature but the circumference gets thinner so average temperature in the domain gets smaller. This is shown in Fig. 11.

VI. CONCLUSIONS

We have studied the thermal distribution of pure blood and an MNP-blood mixture with the effects of non-uniform and uniform magnetic field on them. A computer simulation of the problem was created, and the numerical solution was generated. The results were presented and discussed in detail. To summarize the result of the study:

1. In uniform magnetic field,
 - (a) The highest temperature rises locally at the tip of a fully developed temperature profile.
 - (b) At first, the average temperature does not change much as the magnetic field strength goes up, but over time, it goes down faster than when the magnetic field strength is low.
 - (c) Blood has a tendency to become temporarily less viscous in a high magnetic field. As the Reynolds number increases, it is the temperature. To keep the temperature in

the range between $T_w < T < T_f$, the axial pressure gradient should be kept low, as the Reynolds number increases.

2. In non-uniform magnetic field,
 - (a) Isotherms are pushed in the direction of magnetic force and velocity.
 - (b) When the fluid is less viscous, that is, the Reynolds number is bigger, then the push is more noticeable starting at a lower magnetic strength.
 - (c) Both the average and local maximum temperatures decrease with the increasing magnetic strength.
 - (d) Lower axial pressure gradient is necessary to keep the fluid in therapeutic temperature.
 - (e) $-\frac{\partial T}{\partial y}|_{y=0}$ for $0 \leq x \leq 1$ is proportional to the Reynolds number, axial pressure gradient, and volume fraction.

The three-dimensional model is simplified by our geometric model. Consequently, there are some limitations to our model. A complete three-dimensional model will provide more opportunities to investigate the various types of data. In addition, our calculations assume that the blood and Fe_3O_4 mixture flows as a single phase. A two-phase flow would allow us to study particle dynamics and their respective contributions to the thermal distribution of the fluid under investigation. In the future, we hope to overcome these limitations and examine a more comprehensive model to expand this investigation.

ACKNOWLEDGMENTS

We are thankful to the Ministry of Science and Technology Peoples Republic of Bangladesh for funding this research by NST fellowship grant.

AUTHOR DECLARATIONS

Conflict of Interest

The authors have no conflicts to disclose.

Author Contributions

MD Hassan Faruk: Conceptualization (equal); Data curation (equal); Formal analysis (equal); Investigation (equal); Methodology (equal); Validation (equal); Visualization (equal); Writing – original draft (equal). **Mohammad Ferdows:** Conceptualization (equal); Project administration (equal); Supervision (equal); Writing – review & editing (equal). **E. E. Tzirtzilakis:** Formal analysis (equal); Investigation (equal); Resources (equal); Visualization (equal); Writing – review & editing (equal).

DATA AVAILABILITY

The data that support the findings of this study are available from the corresponding author upon reasonable request.

REFERENCES

- Pauling and C. D. Coryell, "The magnetic properties and structure of hemoglobin, oxyhemoglobin and carbonmonoxyhemoglobin," *Proc. Natl. Acad. Sci. U. S. A.* **22**, 210 (1936).
- E. E. Tzirtzilakis, "A mathematical model for blood flow in magnetic field," *Phys. Fluids* **17**, 0771103 (2005).
- A. Yamagashi, T. Takeuchi, T. Hagashi, and M. Date, "Diamagnetic orientation of blood cells in high magnetic field," *Phys. B: Condense Matter* **177**, 523 (1992).
- C. Corot, P. Robert, J. Idee, and M. Port, "Recent advances in iron oxide nanocrystal technology for medical imaging," *Adv. Drug Delivery Rev.* **58**, 1471 (2006).
- F. Q. Hu, L. Wei, Z. Zhou, Y. L. Ran, Z. Li, and M. Y. Gao, "Preparation of biocompatible magnetite nanocrystals for in vivo magnetic resonance detection of cancer," *Adv. Mater.* **18**, 2553 (2006).
- Y.-X. J. Wang, "Quantitative imaging in medicine and surgery: Progress and perspective," *Quant. Imaging Med. Surg.* **3**, 1 (2011).
- T. Neuberger, B. Schöpf, H. Hofmann, M. Hofmann, and B. von Rechenberg, "Superparamagnetic nanoparticles for biomedical applications: Possibilities and limitations of a new drug delivery system," *J. Magn. Magn. Mater.* **293**, 483 (2005).
- L. H. Reddy, J. Arias, J. Nicholas, and P. Couvreur, "Magnetic nanoparticles: Design and characterization, toxicity and biocompatibility, pharmaceutical and biomedical applications," *Chem. Rev.* **112**, 5818 (2012).
- X. Yang, Y. Chen, R. Yuan, G. Chen, E. Blanco, J. Gao, and X. Shuai, "Folate-encoded and Fe₃O₄-loaded polymeric micelles for dual targeting of cancer cells," *Polymer* **49**, 3477 (2008).
- J. Fortin, C. Wilhelm, J. Servais, C. Menager, J. Bacri, and F. Gazeau, "Size-sorted anionic iron oxide nanomagnets as colloidal mediators for magnetic hyperthermia," *J. Am. Chem. Soc.* **129**, 2628 (2007).
- A. E. Deatsch and B. A. Evans, "Heating efficiency in magnetic nanoparticle hyperthermia," *J. Magn. Magn. Mater.* **354**, 10 (2014).
- P. Hu, L. Kang, T. Chang, F. Yang, H. Wang, Y. Zhang, J. Yang, K.-S. Wang, J. Du, and Z. Yang, "High saturation magnetization Fe₃O₄ nanoparticles prepared by one-step reduction method in autoclave," *J. Alloys Compd.* **728**, 88 (2017).
- R. S. Molday and D. Mackenzie, "Immunospecific ferromagnetic iron-dextran reagents for the labeling and magnetic separation of cells," *J. Immunol. Methods* **52**, 353 (1982).
- A. M. Demin, O. F. Kandarakov, A. S. Minin, D. K. Kuznetsov, M. A. Uimin, V. Y. Shur, A. V. Belyavsky, and V. P. Krasnov, "Modification of chemically and physically obtained Fe₃O₄ magnetic nanoparticles with l-Lys for cell labeling," *Russ. Chem. Bull.* **70**, 1199 (2021).
- Z. Liu, J. Liu, X. Cui, X. Wang, L. Zhang, and P. Tang, "Recent advances on magnetic sensitive hydrogels in tissue engineering," *Front. Chem.* **8**, 124 (2020).
- V. M. Pai, Y. Haik, and C. J. Chen, "Microscopic flow visualization system for fluids in magnetic field," *J. Magn. Magn. Mater.* **194**, 262 (1999).
- K. Khanafer and K. Vafai, "A critical synthesis of thermophysical characteristics of nanofluids," *Int. J. Heat Mass Transfer* **54**, 4410 (2011).
- R. Tao and K. Huang, "Reducing blood viscosity with magnetic fields," *Phys. Rev. E* **84**, 011905 (2011).
- M. A. Teamah and W. M. El-Maghlany, "Augmentation of natural convective heat transfer in square cavity by utilizing nanofluids in the presence of magnetic field and uniform heat generation/absorption," *Int. J. Therm. Sci.* **58**, 130 (2012).
- K. Murase, H. Takata, Y. Takeuchi, and S. Saito, "Control of the temperature rise in magnetic hyperthermia with use of an external static magnetic field," *Phys. Med.* **29**, 624 (2013).
- E. E. Tzirtzilakis and M. A. Xenos, "Biomagnetic fluid flow in a driven cavity," *Meccanica* **48**, 187 (2013).
- E. Voros, M. Cho, M. Ramirez, A. L. Palange, E. De Rosa, J. Key, Z. Garami, A. B. Lumsden, and P. Decuzzi, "TPA Immobilization on iron oxide nanocubes and localized magnetic hyperthermia accelerate blood clot lysis," *Adv. Funct. Mater.* **25**, 1709 (2015).
- M. Sheikholeslami, A. Zeeshan, and A. Majeed, "Control volume based finite element simulation of magnetic nanofluid flow and heat transport in non-Darcy medium," *J. Mol. Liq.* **268**, 354 (2018).
- Y.-D. Tang, R. C. Flesch, C. Zhang, and T. Jin, "Numerical analysis of the effect of non-uniformity of the magnetic field produced by a solenoid on temperature distribution during magnetic hyperthermia," *J. Magn. Magn. Mater.* **449**, 455 (2018).
- Advances in Material Sciences and Engineering, Lecture Notes in Mechanical Engineering* edited by M. Awang, S. S. Emamian, and F. Yusof (Springer, Singapore, 2020).
- T. Elnaqeeb, N. A. Shah, and K. S. Mekheimer, "Hemodynamic characteristics of gold nanoparticle blood flow through a tapered stenosed vessel with variable nanofluid viscosity," *BioNanoSci.* **9**, 245 (2019).
- H. Abdi, S. Y. Motlagh, and H. Soltanipour, "Study of magnetic nanofluid flow in a square cavity under the magnetic field of a wire carrying the electric current in turbulence regime," *Results Phys.* **18**, 103224 (2020).
- H. Badfar, S. Y. Motlagh, and A. Sharifi, "Numerical simulation of magnetic drug targeting to the stenosis vessel using Fe₃O₄ magnetic nanoparticles under the effect of magnetic field of wire," *Cardiovasc. Eng. Tech.* **11**, 162 (2020).
- P. Chandrasekharan, Z. W. Tay, D. Hensley, X. Y. Zhou, B. K. Fung, C. Colson, Y. Lu, B. D. Fellows, Q. Huynh, C. Saayujya, E. Yu, R. Orendorff, B. Zheng, P. Goodwill, C. Rinaldi, and S. Conolly, "Using magnetic particle imaging systems to localize and guide magnetic hyperthermia treatment: Tracers, hardware, and future medical applications," *Theranostics* **10**, 2965 (2020).
- L. S. Sundar, H. M. Abebaw, M. K. Singh, A. M. Pereira, and A. C. Sousa, "Experimental heat transfer and friction factor of Fe₃O₄ magnetic nanofluids flow in a tube under laminar flow at high Prandtl numbers," *IJHT* **38**, 301 (2020).
- K. Venkatadri, A. shobha, C. Venkata Lakshmi, V. Ramachandra Prasad, and B. M. Hidayathulla Khan, "Influence of magnetic wire positions on free convection of Fe₃O₄-water nanofluid in a square enclosure utilizing with MAC Algorithm," *J. Appl. Comput. Appl. Mech.* **51**, 323 (2020).
- R. Pourrajab, A. Noghrehabadi, M. Behbahani, and E. Hajidavaloo, "An efficient enhancement in thermal conductivity of water-based hybrid nanofluid containing MWCNTs-COOH and Ag nanoparticles: Experimental study," *J. Therm. Anal. Calorim.* **143**, 3331 (2021).
- R. E. Rosensweig, *Ferrohydrodynamics* (Courier Corporation, 2014).
- E. E. Tzirtzilakis, V. D. Sakalis, N. G. Kafoussias, and P. M. Hatzikonstantinou, "Biomagnetic fluid flow in a 3D rectangular duct," *Int. J. Numer. Methods Fluids* **44**, 1279 (2004).
- S. M. Mousavi, A. A. R. Darzi, O. A. Akbari, D. Toghraie, and A. Marzban, "Numerical study of biomagnetic fluid flow in a duct with a constriction affected by a magnetic field," *J. Magn. Magn. Mater.* **473**, 42 (2019).
- E. E. Tzirtzilakis, "Biomagnetic fluid flow in an aneurysm using ferrohydrodynamics principles," *Phys. Fluids* **27**, 061902 (2015).
- H. C. Brinkman, "The viscosity of concentrated suspensions and solutions," *J. Chem. Phys.* **20**, 571 (1952).

- ³⁸E. J. Wasp, J. P. Kenny, and R. L. Gandhi, *Solid-Liquid Flow Slurry Pipeline Transportation* (Gulf Publishing Co., 1979).
- ³⁹J. C. Maxwell, *Treatise on Electricity and Magnetism* (Dover Publications, 1954), Vol. 1.
- ⁴⁰COMSOL, Inc., *COMSOL Multiphysics Reference Manual* (COMSOL, Inc., 2020).
- ⁴¹F. Fadaei, M. Shahrokhi, A. M. Dehkordi, and Z. Abbasi, "Heat transfer enhancement of Fe_3O_4 ferrofluids in the presence of magnetic field," *J. Magn. Mater.* **429**, 314 (2017).
- ⁴²R. Saini, S. Vashisth, and R. Bhatia, "Classification of pressure gradient of human common carotid artery and ascending aorta on the basis of age and gender," *Int. J. Comput. Appl.* **145**, 15 (2016).
- ⁴³Z. Abbas and J. Hasnain, "Two-phase magnetoconvection flow of magnetite (Fe_3O_4) nanoparticles in a horizontal composite porous annulus," *Results Phys.* **7**, 574 (2017).
- ⁴⁴C. Kittel, *Introduction to Solid State Physics*, 8th ed. (Wiley, Hoboken, 2005).